International Journal of Bifurcation and Chaos, Vol. 22, No. 2 (2012) 1250027 (12 pages)

DOI: 10.1142/S0218127412500277

QUANTIFYING CHANGES IN THE SPATIAL STRUCTURE OF TRABECULAR BONE

NORBERT MARWAN
Potsdam Institute for Climate Impact Research (PIK), 14412 Potsdam, Germany
Interdisciplinary Center for Dynamics of Complex Systems, University of Potsdam, 14415 Potsdam, Germany
marwan@pik-potsdam.de

GISE BELLER and DIETER FELSENBERG
Charité, Campus Benjamin Franklin, University of Medicine Berlin, 12200 Berlin, Germany

PETER SAPARIN
Department of Biomaterials, Max Planck Institute of Colloids and Interfaces, 14424 Potsdam-Golm, Germany

JÜRGEN KURTHS
Potsdam Institute for Climate Impact Research (PIK), 14412 Potsdam, Germany
Department of Physics, Humboldt University Berlin, 12489 Berlin, Germany

Received December 15, 2011

We apply recently introduced measures of complexity for the structural quantification of distal tibial bone. For the first time, we are able to investigate the temporal structural alteration of trabecular bone. Based on four patients, we show how the bone may alter due to temporal immobilization.

Keywords: 3D medical image analysis; pQCT; trabecular bone; patient immobilization.

1. Introduction

The whole human body is a highly complex and dynamic system ensuring adaptation to a changing environment. Consequently, the human skeletal system is continuously changing in order to adapt its strength especially to current loading conditions. However, in subjects suffering from certain bone diseases, like osteoporosis (loss of bone mineral density and increased fracture risk), limited moveability, or staying in micro-gravity conditions, the bone may change so dramatically that the bone will lose a significant amount of its stability, and fracture risk increases. These changes are on the one hand loss of bone mass, a decrease of the mineralisation of bone, and on the other hand a change in the micro-architecture of the interior bone (trabecular bone). Structural changes in trabecular bone have received much attention in the last years because the loss of bone mass alone cannot explain all variations in bone strength. Moreover, the rapid progress

in high resolution Computed Tomography (CT) imaging facilitates the investigation of the micro-architecture of bone.

The standard method for the quality assessment of the micro-architecture of trabecular bone is histomorphometry [Parfitt *et al.*, 1983; Ito *et al.*, 1998; Hildebrand *et al.*, 1999]. More recent and advanced approaches quantify the complexity of trabecular structures by using measures of complexity based on symbolic dynamics [Saparin *et al.*, 1998; Saparin *et al.*, 2005], recurrence [Marwan *et al.*, 2007a], fractal [Marwan *et al.*, 2007b] or geometric properties [Marwan *et al.*, 2009], or using volumetric spatial decompositions [Stauber & Müller, 2006]. Applying these approaches on 3D images of trabecular bone, it was shown that the micro-architecture changes substantially during the development of osteoporosis. The main conclusions in [Saparin *et al.*, 2005; Marwan *et al.*, 2007b; Marwan *et al.*, 2009] were that the complexity of the bone micro-architecture decreases in the course of bone loss whereas the volume and surface of the trabecular structure changes by a different amount. This latter conclusion confirms former findings that the shapes of the trabeculae change during bone loss (e.g. from plate-like structure to rod-like structure) [Hildebrand *et al.*, 1999].

In this study, we apply recently developed measures of complexity to characterize for the first time the temporal change of complex spatial structures of trabecular bone. We analyze the changes of the three-dimensional micro-architecture of distal tibia of patients who suffered from temporal immobilisation due to a disease or an accident on the left body side. Moreover, we investigate the effects of errors in positioning the volume of interest within the bone during the follow-up CT scans and of choosing different segmentation parameters.

2. Data and Methods

For our analysis, we have used data from the *Advanced Detection of Bone Quality* (*ADOQ*) study. In this framework, different subject groups were investigated in order to develop reference data for high-resolution 3D peripheral Quantitative Computer Tomography (3D-pQCT). It includes 3D data from patients suffering from ligament rupture or fracture of the extremity, or from hemiplegic patients (half of the body is paralysed).

For each patient the 3D-pQCT investigations were performed over a period of six months including baseline imaging and four follow-up measurements with an interval of six weeks. The measurements were performed at all extremities: left and right distal radii and distal tibiae. In our investigation, we focused on distal tibia. We have selected four patients, who have attended the follow-up measurements at least three times, and who had suffered temporal immobility due to a disease or an accident on the left body side.

The data were acquired *in vivo* by XtremeCT 3D-pQCT scanner (Scanco Medical AG, Switzerland). The 3D-pQCT images have an isotropic voxel size of 82 μm, the image matrix has a size of 1536 voxels $\times$ 1536 voxels $\times$ 110 voxels (length of the imaged region along the bone axis was 9.02 mm; Fig. 1). The clinical situation of the remaining patients is summarised in Table 1.

The pQCT images were converted from 3D-pQCT data format into a 3D mesh format for our analysis using the Amira software platform (Mercury Computer Systems Inc.).

The comparison of follow-up 3D-pQCT scans was done by considering the common regions overlapping in all scans (see also Sec. 3.1). This was necessary because the scan at different time points causes slight displacements of the imaged regions of distal tibia. To minimize deviations due to dislocations/displacements, the pQCT device establishes common regions for all of the scans. However, small tilts cannot be corrected with this method, hence leading to potential variations in structural analysis.

For the quantification of the bone microarchitecture we focus only on the trabecular part of the bone. Therefore, to separate the trabecular bone from the rest of the imaged 3D data we created manually volumes of interest (VOI). Then, in order to reduce the level of noise in the pQCT data, the 3D images were filtered using a 3D median filter. Bone and marrow voxels were separated by using of a global thresholding; the threshold level was set to 2800 units of the pQCT image (this value was found heuristically by looking at the histogram of the attenuation values, but also see Sec. 3.2).

At first, we calculated the classical measure bone volume fraction BV/TV which provides information about the amount of bone material. Then we calculated recently introduced structural measures of complexity (SMCs), which are based on symbol encoding, curvature, translational invariance and

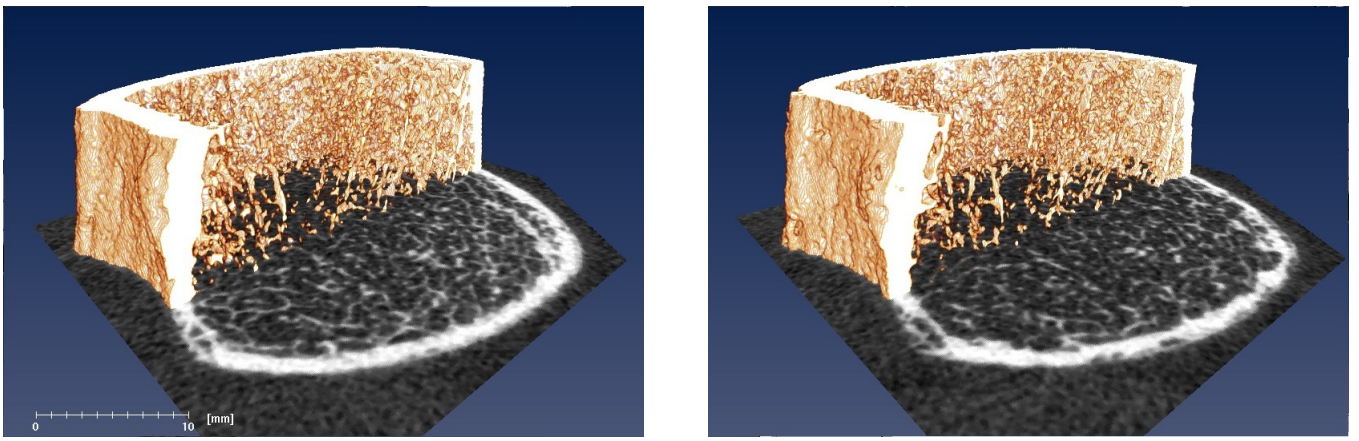

(a) (b)

Fig. 1. 3D-pQCT images of left distal tibia of patient 9 (a) at the beginning of the study and (b) after four months at the end of the study showing slight variations of the bone micro-architecture. The lower, gray-scale plane represents a 2D orthoslice, and the colored volume rendering shows a cut part of the 3D image.

local shape of trabecular bone elements (Table 2) [Saparin *et al.*, 2005; Marwan *et al.*, 2005, 2007b, 2009].

SMCs based on symbol encoding use a limited set of structural elements or symbols for the quantification of the 3D structures. The purpose of the symbol-encoding procedure is to reduce the amount of information in a 3D-pQCT image to its essential structural composition by representing the bone architecture. The modified symbol-encoding procedure for the micro-CT data is based on an alphabet of three different symbols: M, marrow voxel; I, internal bone voxel; and S, surface bone voxel. Bone "surface" is a one voxel-thick layer of bone voxels which lie at the boundary between two tissues: bone and marrow. Based on distributions and joint distributions of the symbols, the measures of complexity are defined. For example, the surface complexity index SurfCI is defined by

$$\mathrm{SurfCI} = -\sum_{\mathrm{VOI}} p_{\mathrm{surf}} \log_2 p_{\mathrm{surf}}, \tag{1}$$

with p_{surf} as the distribution of local surface indices

$$p_{\mathrm{surf}} = \frac{p_{\mathrm{loc}}(S)}{p_{\mathrm{loc}}(I) + p_{\mathrm{loc}}(S)}. \tag{2}$$

This measure is calculated in a small moving cubic box. SurfCI assesses the complexity of the distribution of bone surface voxels in 3D. Other SMCs based on symbol encoding quantify the complexity or the distribution of the trabecular structures [Saparin *et al.*, 2005].

The main idea behind the SMCs based on the geometrical shape depends on the fact that different 3D objects of the same volume have different surfaces, depending on their geometrical shape. For example, a long cylinder (length is much larger than radius) has a larger surface than a cube of the same volume, whereas a sphere has the smallest possible surface for the same given volume. Therefore, the ratio between volume and surface is used in the definition of several SMCs, like the local shape index

$$\sigma_{\mathrm{loc}} = \frac{S_{\mathrm{bone}}}{S_{\mathrm{sphere}}} \quad \text{with } S_{\mathrm{sphere}} = 6\sqrt[3]{\pi \hat{V}_{\mathrm{bone}}^2}, \tag{3}$$

where S_{bone} is the surface of trabecular bone in a small box, V_{bone} is its volume, and S_{sphere} is the smallest possible surface for such volume (which corresponds to the surface of a sphere). The average of the local shape index ASHI, as well as the measures SHC and MISH, are able to distinguish

Table 1. Diagnosis of the four patients whose tibial bone structure was imaged by 3D-pQCT and assessed by the structural measures of complexity.

Patient ID	Clinical Diagnosis	Follow-Up Visits
5	Medial fracture on the left femoral neck	5
9	Ligament rupture left knee	4
11	Media infarct (stroke) with left-sided failure/strong distal paralysis, caused wheel-chair dependence	3
14	Impression fracture on the left tibial plateau	4

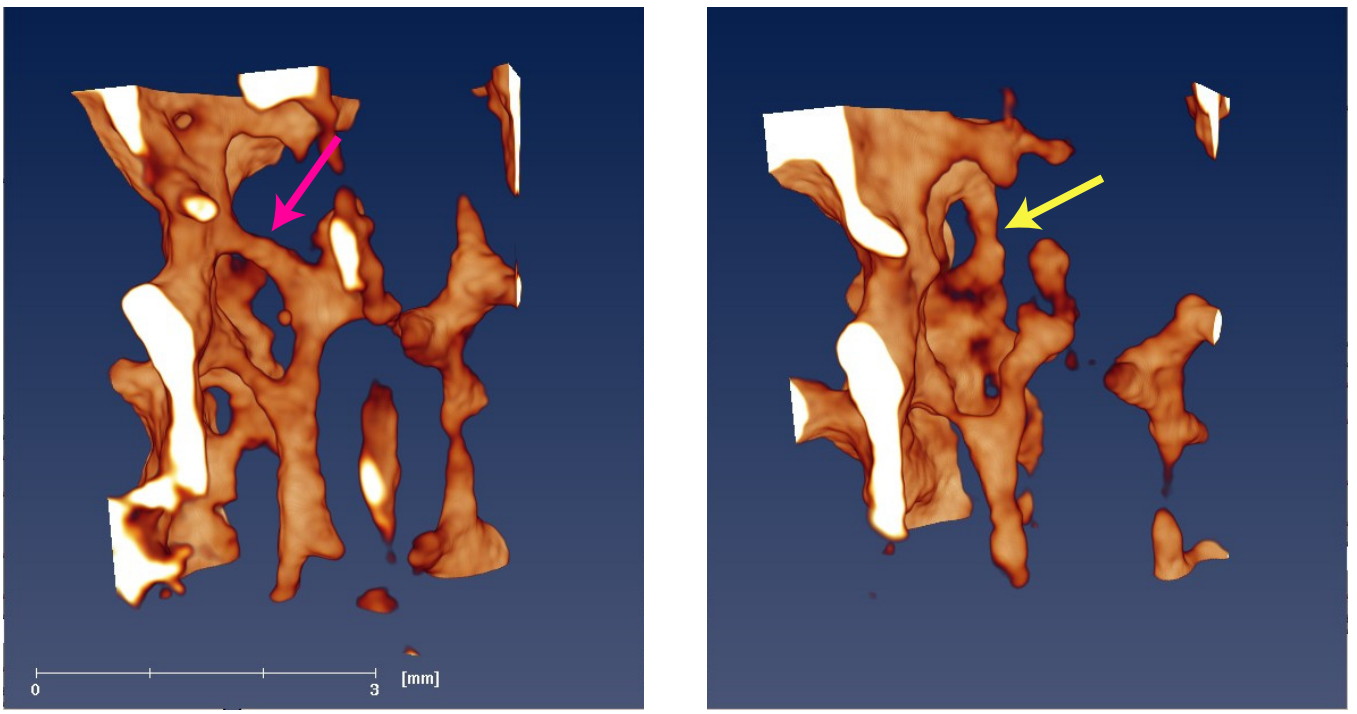

(a) (b)

Fig. 2. A detail of the 3D-pQCT image shown in Fig. 1, (a) at the beginning of the study and (b) after four months at the end of the study. The thinning and resorption of trabeculae is visible (magenta arrow). But new trabeculae can also appear (yellow arrow).

between different shapes with the same volume but whose surface differ, like plates and rods. MCE and MCC quantify the complexity of the bone surface [Marwan *et al.*, 2009].

Further measures are based on fractal properties, translational invariance and small-scale spatial auto-correlation. For example, the lacunarity Λ measures the variation of the bone fraction in small moving boxes by using the ratio of the second and first moments of the distribution $n(s, r)$ of the bone density:

$$\Lambda(r) = \frac{\mu_2(r)}{\mu_1^2(r)}, \tag{4}$$

Table 2. Structural measures of complexity (SMCs) used in this study.

SMCs based on symbol encoding [Saparin *et al.*, 1998; Saparin *et al.*, 2005]	3D Normalized Entropy of geometrical locations of bone tissue	S_n
	Structure Complexity Index, based on bone volume fraction	$\mathrm{SCI}_{\mathrm{BV/TV}}$
	3D Structure Complexity Index	$\mathrm{SCI}_{\mathrm{3D}}$
	Surface Complexity Index	SurfCI
	Surface Index of Global Ensemble	SurfIGE
Measures based on local shape and curvatures [Marwan *et al.*, 2005; ESA MAP team AO-99-030, 2005; Marwan *et al.*, 2009]	Shape Complexity	SHC
	Averaged Shape Index	ASHI
	Shape Mutual Information	MISH
	Marching Cubes Entropy Index	MCE
	Marching Cubes Complexity	MCC
	Total curvature	K
	Mean curvature	H
Measures assessing translational invariance [Marwan *et al.*, 2007b]	Lacunarity	Λ
	Morans's I index	I

where the first and second moments are

$$\mu_1(r) = \frac{1}{N}\sum_s sn(s,r) \quad \text{and}$$
$$\mu_2(r) = \frac{1}{N}\sum_s s^2 n(s,r), \tag{5}$$

N is the total number of boxes, s the local bone density and r is the size of the moving box [Marwan *et al.*, 2007b]. The lacunarity measures therefore how homogenously distributed the trabecular bone is.

As we have mentioned, several SMCs are based on the analysis of ensembles of local properties estimated from a moving cubic box. The size of the moving cubic box should be small enough to locally quantify structural elements, but large enough to cover a sufficient surface necessary to distinguish between different shapes and to reduce artefacts. Based on this requirements, we have found empirically a trade-off for the box size to be $20 \times 20 \times 20$ voxels ($1.64 \times 1.64 \times 1.64$ mm).

The SMCs have been calculated on the trabecular bone of the distal tibia within the specified VOI. As the same bone region was scanned at six weeks intervals, for the first time the results allow us to study structural changes in the same trabecular bone over time.

3. Experiments to Test Stability and Reproducibility of the Structural Measures

Stability and reproducibility of the measures are crucial requirements to any data analysis tools. In the following we present our studies of the influence of main disturbing factors, including mismatch of VOIs and different bone segmentation thresholds. In another study, we have investigated the effects of the image resolution [Marwan *et al.*, 2009].

3.1. *Local mismatch of VOI or common region*

For the study of structural changes during time, the 3D-pQCT images of the distal tibia have to be acquired at exactly the same location in order to provide images of bone appropriate for longitudinal evaluation. Therefore, the software of the pQCT device calculates the common region between consecutive images. Nevertheless, small deviations in the positioning of the common region still remain, e.g. due to tilts. Therefore, we analyzed the variation of the SMCs for an artificial dislocation of the VOI.

In this numerical experiment we used 3D-pQCT data of the left distal tibia from patient with ID 9. We reduced the original VOI by removing a small 82 μm thick volume at its perimeter (that was defined as 1 voxel from each side on the xy-plane) and applied small random local displacements of the VOI in the xy-plane in the interval of ± 0.95 voxels (corresponding x- and y-shifts were randomly distributed uniformly between -77 and $77\,\mu$m). The calculations were repeated 500 times in order to get distributions of the measures from randomly displaced volume of interest (Table 3).

Due to the random shifts by maximal of one voxel, the variation range of the SMCs was between 0.65% (S_n) and 37.0% (H). As a variation range we consider here the distance between the 5%- and 95%-quantiles normalized by the median value of the measure. Therefore, this performance measure allows us to assess the influence of the local displacement on the SMCs. We find that the measures BV/TV, the curvatures H and K as well as Λ are rather sensitive to the displacement with variation ranges above 10%. In contrast, the measures $\mathrm{SCI}_{\mathrm{BV/TV}}$, SurfCI, S_n, ASHI, MISH, SHC

Table 3. Median and variation range of the structural measures of complexity for small random local displacements of VOI in interval from ± 77 μm (corresponding approximately to less than one voxel). The results are obtained from 500 realizations of random displacements of the VOI in CT images of distal tibia of patient ID 9.

Measure	Median	Std. Deviation	$q_{0.05}$	$q_{0.95}$	Range (%)
BV/TV	0.22	0.01	0.20	0.23	13.14
$\mathrm{SCI}_{\mathrm{3D}}$	0.76	0.01	0.73	0.77	4.39
$\mathrm{SCI}_{\mathrm{BV/TV}}$	0.90	0.01	0.89	0.91	2.37
SurfCI	0.86	0.01	0.84	0.86	2.22
SurfIGE	0.70	0.03	0.69	0.75	9.39
S_n	0.93	0.00	0.93	0.93	0.65
H	1.03	0.15	0.91	1.29	37.01
K	-1.88	0.10	-2.08	-1.75	17.59
Moran's I	0.75	0.01	0.73	0.75	3.23
Λ	0.41	0.03	0.35	0.43	19.36
ASHI	1.73	0.01	1.73	1.76	1.70
MISH	0.19	0.00	0.19	0.19	1.14
SHC	0.22	0.00	0.22	0.23	2.99
MCC	5.72	0.03	5.67	5.75	1.28
MCE	0.65	0.01	0.64	0.67	4.83

and MCC are much less sensitive, below 3%. The remaining measures, SCI_{3D}, SurfIGE, Moran's I and MCE are slightly more sensitive with the variation range around 5%.

These are crucial findings, because they imply that we cannot interpret as significant the relative variations in the range below 5% (that is, a half of the maximal range of 10% found in our simulations) in such measures as BV/TV and SurfIGE, and even variations around 10–20% in the curvatures H, K as well as Λ, as reflection of real structural changes, since it is impossible to exclude positioning errors due to the minor shifts of the VOI during consecutive CT measurements. In the interpretations of the results derived from the ADOQ data in Sec. 4 we will take into account these error ranges.

Next, we have compared the SMCs calculated from the entire 3D-pQCT images and the measures obtained from the common regions that match at different time-points. After evaluating the structure in the common regions, we have repeated the calculations of the SMCs for left distal tibia of patients with ID 5 and 9 for the entire trabecular VOIs that are larger than the common regions of the same measurements. The differences in results derived from the common region and the entire trabecular VOI are rather small for most of the SMCs (Table 4). In general, the typical trend in the behavior of the measures found in matched regions remains the same when the entire VOIs are analyzed (Fig. 3). Remarkable differences in the changes in time occur for measures SCI_{3D} (only patient 5), SurfIGE, MISH (only patient 5, see Fig. 4), MCE and Moran's I index. Large differences in the absolute values were found in MISH, H and K. However, for H and K the trend remains very similar when the matching regions and the entire trabecular VOI are compared.

Table 4. Maximal and mean relative differences between the structural measures calculated for common region and for the entire vertebral VOI of the images of patients ID 5 and 9.

	Patient No. 5		Patient No. 9	
Measure	Max. Dev. (%)	Mean Dev. (%)	Max. Dev. (%)	Mean Dev. (%)
BV/TV	2.4	1.4	3.8	2.6
SCI_{3D}	1.5	0.9	0.9	0.6
$SCI_{BV/TV}$	0.5	0.3	0.6	0.4
SurfCI	1.1	0.7	1.0	0.6
SurfIGE	4.0	2.3	4.0	2.5
S_n	0.1	0.0	0.1	0.0
H	11.3	7.1	11.0	6.5
K	33.3	21.3	19.3	13.1
Moran's I	0.9	0.5	1.2	0.8
Λ	2.8	1.4	2.7	1.7
ASHI	1.1	0.7	0.4	0.3
MISH	21.8	16.9	0.4	0.3
SHC	6.3	4.6	0.8	0.6
MCC	0.8	0.5	0.3	0.2
MCE	2.3	1.4	2.1	1.4

3.2. *Dependence on the segmentation threshold*

The choice of the bone segmentation threshold is an important step in the evaluation of bone

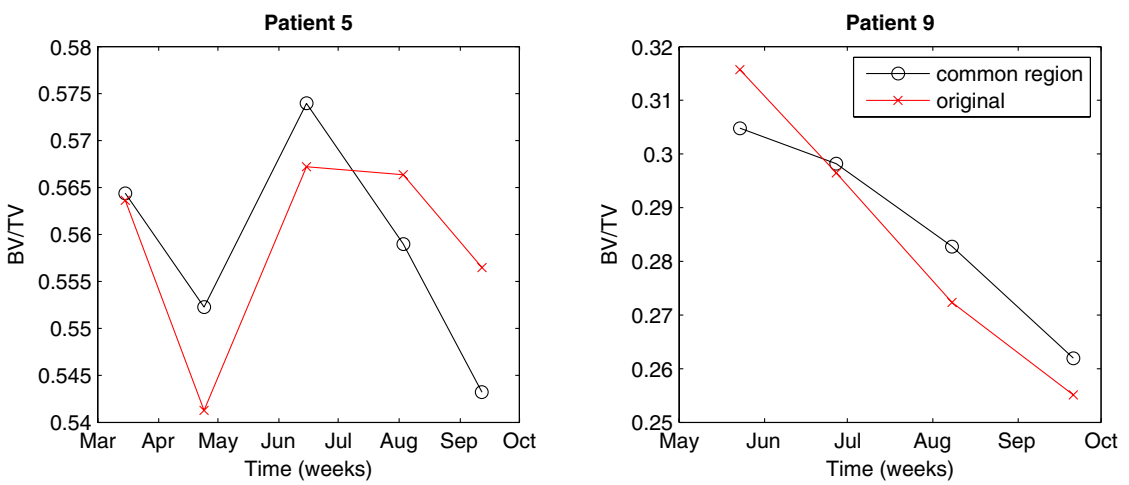

Fig. 3. The BV/TV calculated from the entire trabecular VOIs and the common regions of left distal tibiae for patients 5 and 9.

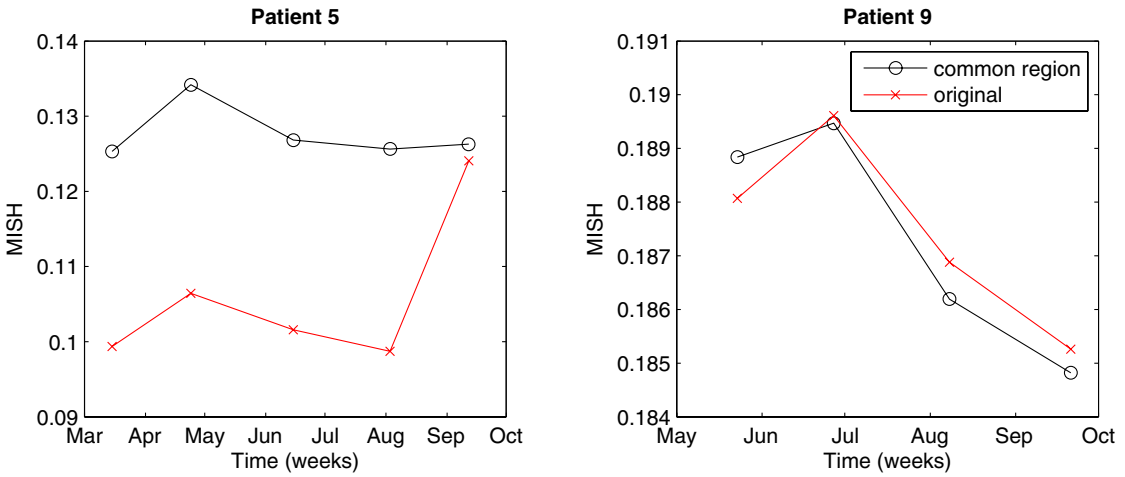

Fig. 4. The shape mutual information MISH calculated from the entire trabecular VOIs and the common regions of left distal tibiae for patients 5 and 9.

architecture. Therefore, we have studied how the choice of segmentation threshold affects the different SMCs. For this experiment we have used the 3D-pQCT images from patient 5. The bone segmentation threshold was set to values of $2300, 2800, 3200$ and 4000 according to a threshold value correspondingly set too low, optimal value, too high, and extremely high.

We found that absolute values of all SMCs depend on the segmentation thresholds. For some measures like SCI_{3D}, $\mathrm{SCI}_{BV/TV}$, K and Λ, their absolute values for the extreme thresholds 2300 and 4000 differ much from the values of the thresholds 2800 and 3200 (Fig. 5). For several measures, as BV/TV, SCI_{3D}, $\mathrm{SCI}_{BV/TV}$, SurfCI, S_n, H, K, Λ, MISH and MCC we found a different trend only for the extreme low and extreme high threshold levels, whereas for levels of 2800 and 3200, the trend remained similar. Similar evolution in time were found for the other measures SurfIGE, Moran's I, ASHI, SHC and MCE indicating that the trend (or qualitative behavior) of these measures is not as sensitive to the choice of the threshold as of the other measures (Fig. 6). Large differences for the longitudinal behavior, and hence high sensitivity, were found for the measures H, K and MCC.

These results confirm that our choice of the bone segmentation threshold at the level of 2800 is appropriate, because more extreme threshold values like 2300 or 4000 reveal more different results (but in the same direction). Moreover, this numerical experiment demonstrates that a slight change of the

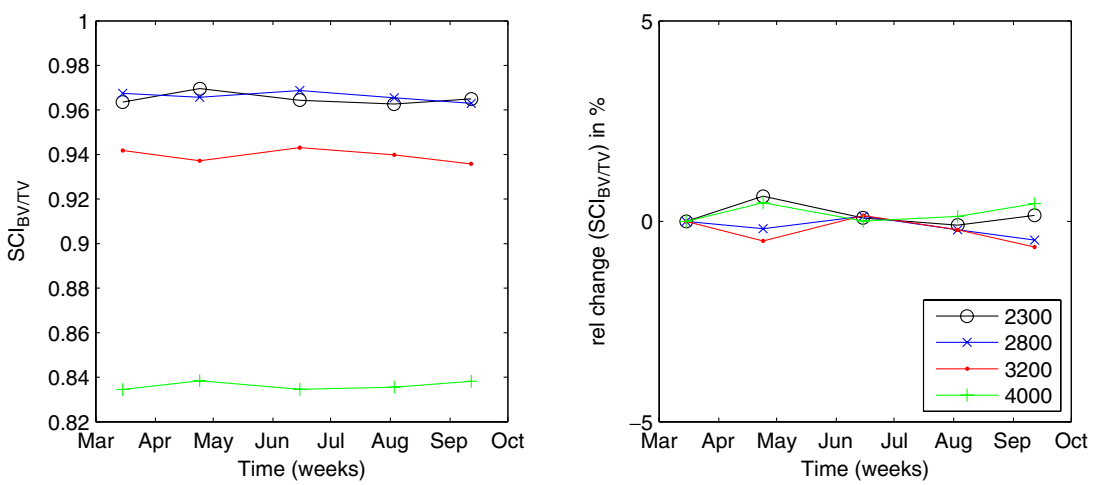

Fig. 5. Exemplary SMC shown for different values of bone segmentation threshold reveals large difference in the absolute values of the threshold level sets that are extremely high (here 4000 pQCT units) or low (2300 pQCT units).

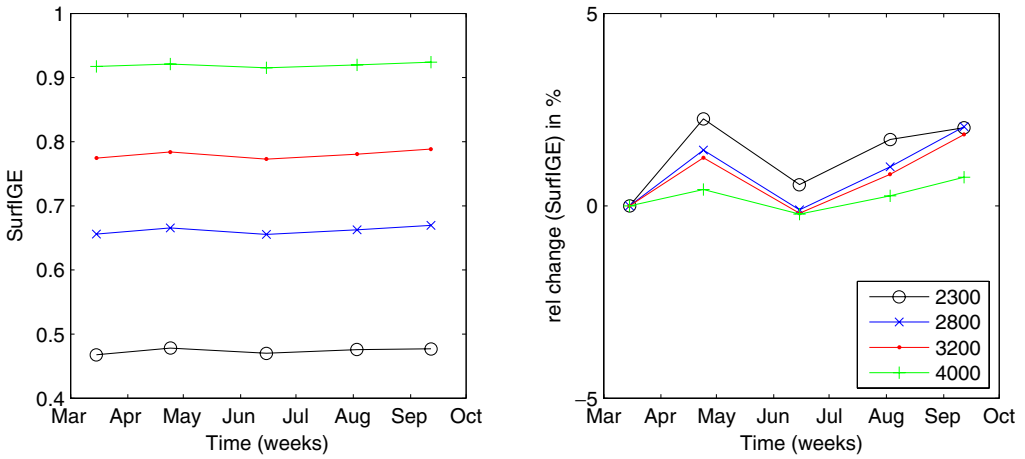

Fig. 6. Exemplary SMC shown for different values of bone segmentation threshold reveals different absolute values but same qualitative behavior.

threshold would not affect the qualitative findings of how the SMCs evolve with time.

4. Evaluation of 3D-pQCT Data from ADOQ Study

The set of 3D structural measures of complexity was applied to evaluate the architectural changes of trabecular bone in patients of temporal immobility, imaged by 3D-pQCT obtained during the ADOQ study. In order to compare SMCs with classical histomorphometry, we used the trabecular thickness Tb.Th. The findings with regards to the stability and reproducibility of the structural measures reported in Sec. 3 were used to validate the range if changes of the SMCs have been found in the longitudinal study (except the Tb.Th, because this measure was calculated directly by the pQCT device). The results of the evaluation are shown in Figs. 7–11.

Considering the BV/TV of all the four analyzed patients and comparing the left and right distal tibiae, we observe bone degradation in patients 5 and 9, whereas the BV/TV for patients 11 and 14 remained almost constant (Fig. 7). This is especially surprising for patient 11, because after a stroke he was partly disabled and needed a wheelchair. Most likely the rehabilitation therapy after the stroke was very effective. In contrast, patient 9 experienced a clear decrease in BV/TV, in particular on the

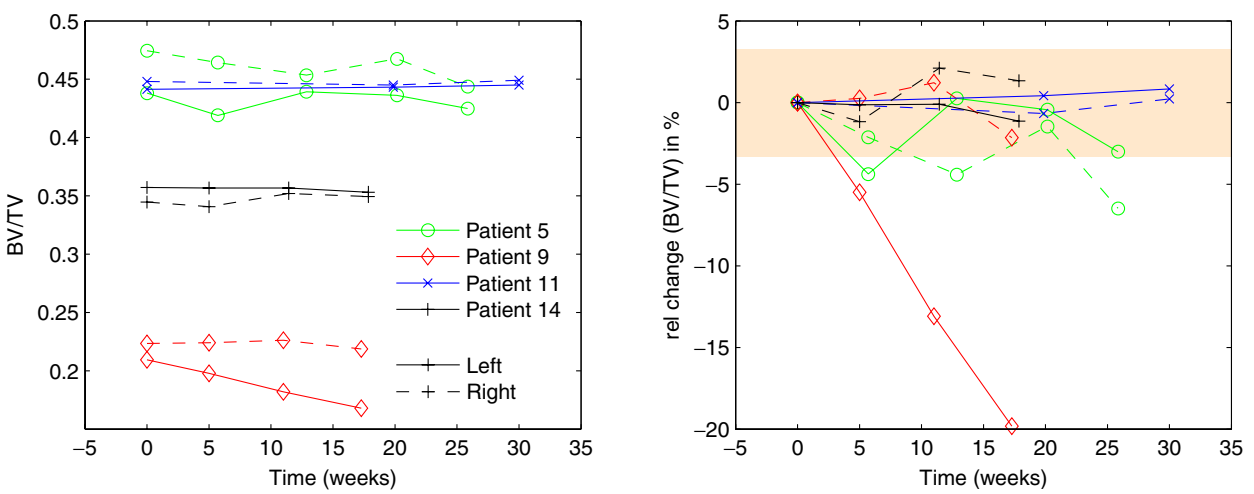

(a) (b)

Fig. 7. Bone volume fraction BV/TV expressed (a) in % and (b) its relative change during the consecutive measurements after trauma or disease caused immobility of the left limb. The rose-shaded region marks the range of variation caused by positioning errors.

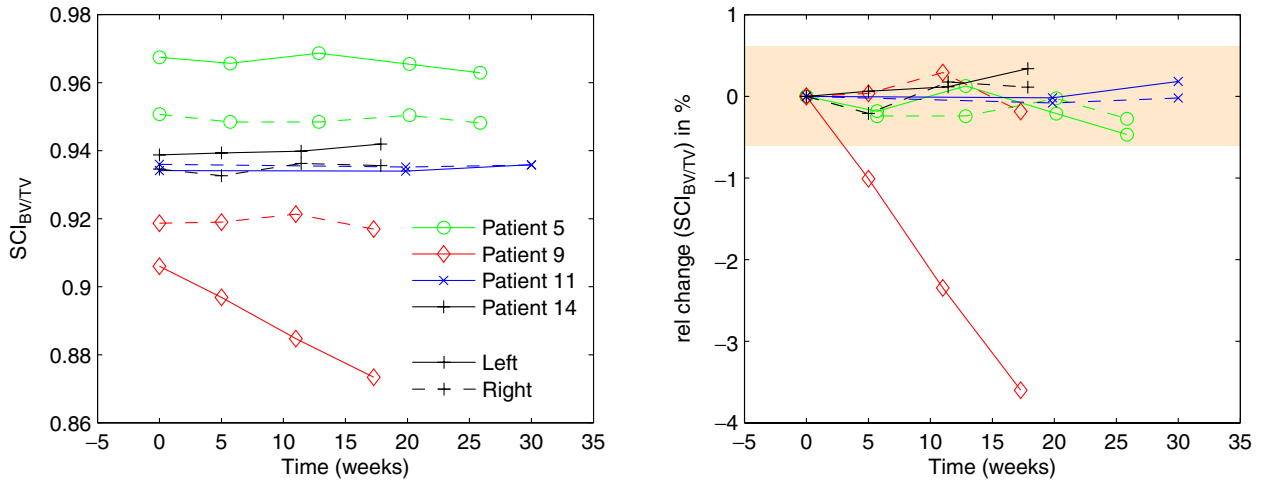

(a) (b)

Fig. 8. Structural complexity measured (a) by $\mathrm{SCI}_{\mathrm{BV/TV}}$ and (b) its relative change during the consecutive measurements after trauma/disease caused immobility of the left limb. The rose-shaded region marks the range of variation caused by positioning errors.

left distal tibia, probably because the patient saved his left leg. The BV/TV of the patient 5 tibiae decreased slightly.

For **patient 11** (left-sided paralysis after stroke), we found that all measures did not change significantly during the investigated interval (see Figs. 7–11). Except for ASHI and MISH, whose range of change is rather small, all relative changes remained within the range of measurement-to-measurement variability due to positioning of the VOI. Moreover, from our analysis we can conclude that this patient (as well as patient 5) had probably the strongest bone among all considered patients: BV/TV of patients 11 and 5 had the highest values, its trabecular architecture was very complex, as it is indicated by high $\mathrm{SCI}_{\mathrm{3D}}$, the mean curvature H is lowest (and even negative), ASHI has lowest values suggesting more convex trabecular structure, what is typical for a dense trabecular bone. From the viewpoint of bone morphometry, the proximal tibiae of patient 11 are also characterized by the highest Tb.Th (Fig. 11).

Patient 14 (impression fracture left tibial plateau) has an intermediate level of bone volume

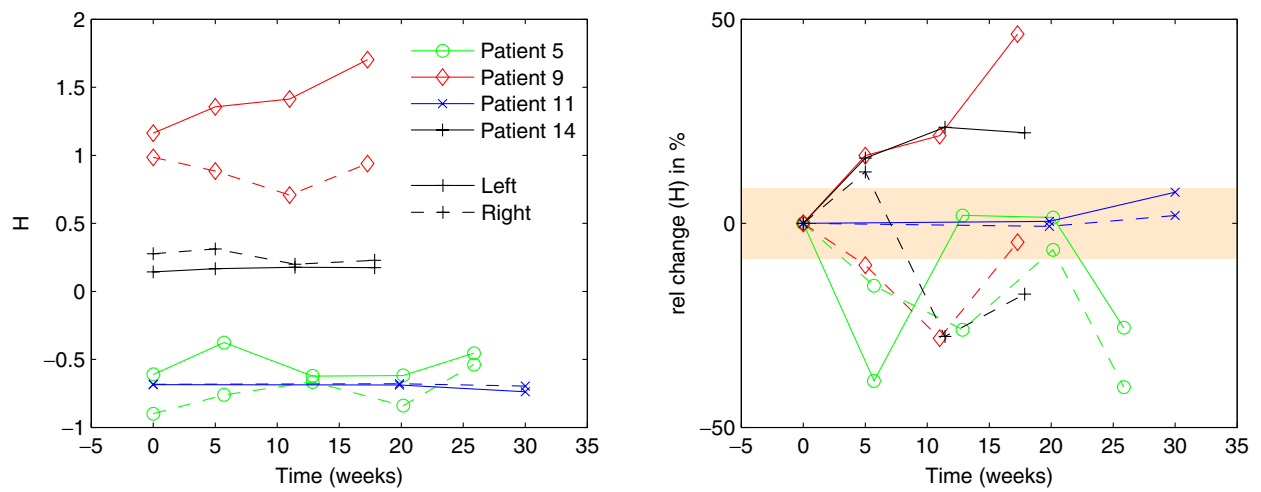

(a) (b)

Fig. 9. (a) Mean curvature H (in mm^{-1}) and (b) its relative change during the consecutive measurements after trauma/disease caused immobilty of the left limb. The rose-shaded region marks the range of variation caused by positioning errors.

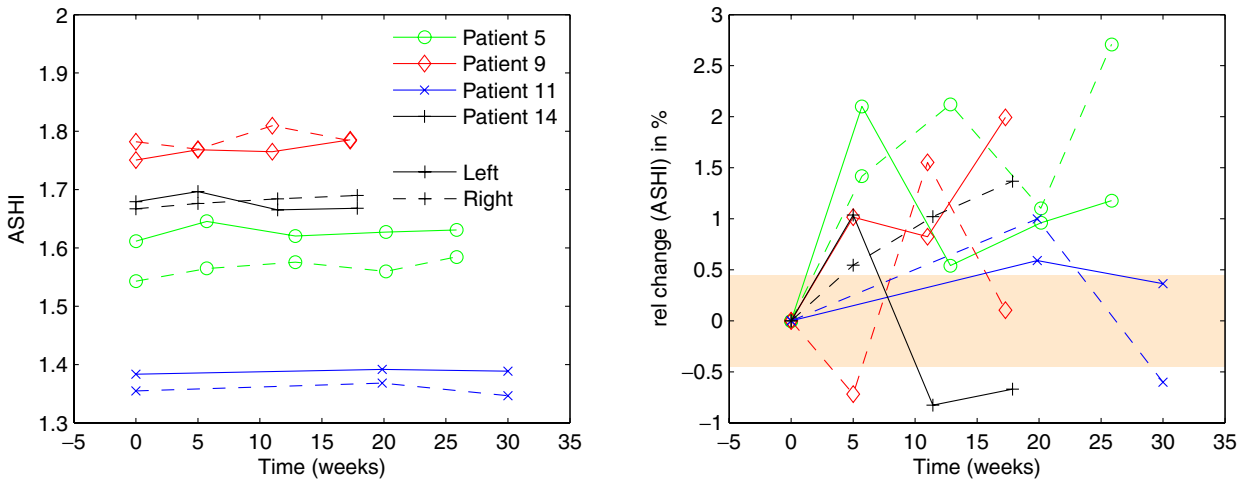

(a) (b)

Fig. 10. Shape complexity measured (a) by ASHI and (b) its relative change during the consecutive measurements after trauma/disease caused immobility of the left limb.

fraction and complexity of trabecular bone structure (Figs. 7–11). For this patient, most of the measures were values between the extreme values of patients 9 and 11. However, during the investigated period of time, the trabecular bone did not change much as indicated by the structural measures which vary only within their error range. We found a slight increase of the surface complexity of the affected left distal tibial trabecular bone after week 10, as revealed by the measures SurfCI, S_n, ASHI and SHC (all $< 1\%$). Moreover, the mean curvature H increased slightly, suggesting a small amount of thinning of the trabeculae.

The SMCs for **patient 5** (fracture on the left femoral neck) reveal that this patient had also strong bone, as observed by high bone density, high complexity of the trabecular architecture, and low values of the mean curvature H (that is also negative). During the investigation period, the trabecular bone composition was only slightly changing (Figs. 7–11). The bone density decreased up to -5%, the structural complexity as quantified by SCI_{3D} decreased only by -2%, and the variability of local trabecular shapes decreased (measured by an increase of ASHI by 2.5%, MISH by 15%, and a decrease of SHC by -7%). H varied

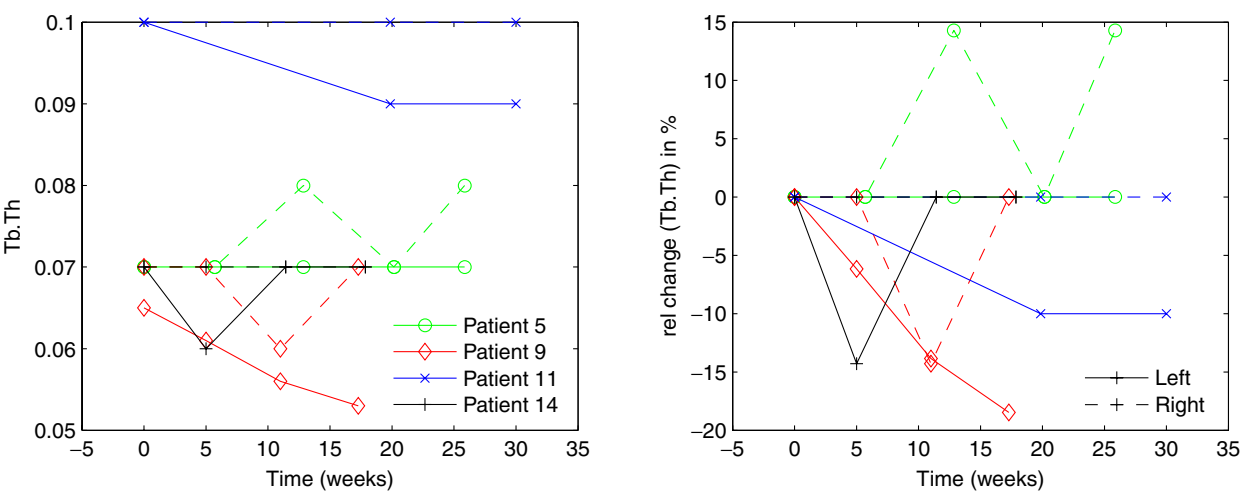

(a) (b)

Fig. 11. (a) Trabecular thickness Tb.Th (in mm) and (b) its relative change during the consecutive measurements after trauma/disease caused immobility of the left limb.

during the investigated period, but finally increased (25%). The other measures vary only slightly or do not allow reliable interpretations because the range of variations is within the measurement-to-measurement error range. Nevertheless, it is remarkable that the left and right sides seem to be affected in a similar way; the structural measures vary on both sides with same amplitudes. However, for several measures we found anti-correlation between the values obtained from the left and right sides (e.g. in BV/TV, SCI_{3D}, total curvature K, ASHI or MCE). This could be caused by an alternative loading of the left and the right sides (starting with the right because the left side suffered the fracture).

In contrast, **patient 9** (ligament rupture) turned out to be the patient with lowest bone density and lowest complexity of the trabecular microarchitecture. This patient experienced a dramatic degradation of trabecular bone as expressed by a decrease of bone volume fraction (up to -20%) and significant changes of the trabecular structure during the investigation period of 17 weeks, in particular on the left side (which was the affected side by the ligament rupture; see Figs. 7–11). The thinning of the trabeculae is well expressed by the increase of the mean curvature H (50%) and the decrease of Tb.Th (-20%). The structural complexity as quantified by SCI_{3D} decreased by -7% (this change is also confirmed by the other SMCs like $SCI_{BV/TV}$, SurfCI, and SurfIGE). The degradation of the trabecular structure caused an increase of the variability of the local shape of bone's structural elements, expressed by a decreasing of MISH by -4%.

5. Conclusions

We have applied recently introduced structural measures of complexity (SMC), which are based on symbol encoding, curvature, translational invariance and local shape of trabecular bone elements, to trabecular bone structure in distal tibia. For the first time, we have been able to study temporal alterations in 3D trabecular bone structure using SMCs.

The developed SMCs are able to detect and assess the temporal alterations in the trabecular bone structure in distal tibia due to temporal immobility. The detected structural variations have been different from subject to subject due to different diseases or sites of the fractures, as well as different treatments. For two patients the range of change of some measures was smaller than their measurement-to-measurement variability range due to the errors in positioning of the imaged part of the tibia, suggesting a positive effect of the preventive treatment. The developed SMCs based on the shape index are sensitive to structural changes; their range of change is significant and exceeds the interval of measurement-to-measurement variation due to different positioning of the analyzed limb.

Moreover, we have investigated the effect of small displacements of the imaged volume during the pQCT scan and the influence of different bone segmentation thresholds. Using simulations of artifical position errors of the volume of interest we have been able to define a 95% variation (confidence) level for the SMCs. In the future, the SMCs will be further systematically studied by applying models for bone remodeling (e.g. [Huiskes *et al.*, 2000; Weinkamer *et al.*, 2004; Rusconi *et al.*, 2008]).

Our findings support that the recently proposed SMCs are useful to investigate trabecular bone alterations [Saparin *et al.*, 2005; Marwan *et al.*, 2005; Marwan *et al.*, 2007b; Marwan *et al.*, 2009]. This study has demonstrated their abilities to quantify longitudinal changes. In particular, they can be applied in clinical diagnosis or monitoring when 3D-pQCT imaging is available.

Acknowledgments

This study was co-funded by the Microgravity Application Program/Biotechnology from the Human Spaceflight Program of the European Space Agency (project MAP AO-2004-125), by the European Commission ADOQ study (Contract QLK-CT-2002-02363, Key action No. 6) and the Swiss government, and received support from Siemens AG and Scanco Medical AG. We thank Hans-Chrisian Hege and Steffen Prohaska, Zuse Institute Berlin (ZIB), for the support and help with the Amira software, as well as Jesper Skovhus Thomsen, Peter Fratzel and Wolfgang Gowin for fruitful discussions.

References

ESA MAP team AO-99-030 [2005] "Assessment of bone structure and its changes in microgravity," *SP-1290 Microgravity Applications Programme: Successful Teaming of Science and Industry* (ESA publications division, ESTEC, Noordwijk), pp. 282–305.

Hildebrand, T., Laib, A., Müller, R., Dequeker, J. & Rüegsegger, P. [1999] "Direct three-dimensional morphometric analysis of human cancellous bone: Microstructural data from spine, femur, iliac crest, and calcaneus," *J. Bone Miner. Res.* **14**, 1167–1174.

Huiskes, R., Ruimerman, R., van Lenthe, G. H. & Janssen, J. D. [2000] "Effects of mechanical forces on maintenance and adaptation of form in trabecular bone," *Nature* **405**, 704–707.

Ito, M., Nakamura, T., Matsumoto, T., Tsurusaki, K. & Hayashi, K. [1998] "Analysis of trabecular microarchitecture of human iliac bone using microcomputed tomography in patients with hip arthrosis with or without vertebral fracture," *Bone* **23**, 163–169.

Marwan, N., Saparin, P., Thomsen, J. S. & Kurths, J. [2005] "An innovative approach for the assessment of 3D structures in trabecular bone," *J. Gravitat. Physiol.* **12**, 127–128.

Marwan, N., Kurths, J. & Saparin, P. [2007a] "Generalised recurrence plot analysis for spatial data," *Phys. Lett. A* **360**, 545–551.

Marwan, N., Saparin, P. & Kurths, J. [2007b] "Measures of complexity for 3D image analysis of trabecular bone," *The European Phys. J. — Special Topics* **143**, 109–116.

Marwan, N., Kurths, J., Thomsen, J. S., Felsenberg, D. & Saparin, P. [2009] "Three dimensional quantification of structures in trabecular bone using measures of complexity," *Phys. Rev. E* **79**, 021903.

Parfitt, A. M., Mathews, C. H. E., Villanueva, A. R., Kleerekoper, M., Frame, B. & Rao, D. S. [1983] "Relationships between surface, volume, and thickness of iliac trabecular bone in aging and in osteoporosis," *J. Clin. Invest.* **72**, 1396–1409.

Rusconi, M., Zaikin, A., Marwan, N. & Kurths, J. [2008] "Effect of stochastic resonance on bone loss in osteopenic conditions," *Phys. Rev. Lett.* **100**, 128101.

Saparin, P. I., Gowin, W., Kurths, J. & Felsenberg, D. [1998] "Quantification of cancellous bone structure using symbolic dynamics and measures of complexity," *Phys. Rev. E* **58**, 6449.

Saparin, P. I., Thomsen, J. S., Prohaska, S., Zaikin, A., Kurths, J., Hege, H.-C. & Gowin, W. [2005] "Quantification of spatial structure of human proximal tibial bone biopsies using 3D measures of complexity," *Acta Astronautica* **56**, 820–830.

Stauber, M. & Müller, R. [2006] "Age-related changes in trabecular bone microstructures: Global and local morphometry," *Osteop. Int.* **17**, 616–626.

Weinkamer, R., Hartmann, M. A., Brechet, Y. & Fratzl, P. [2004] "Stochastic lattice model for bone remodeling and aging," *Phys. Rev. Lett.* **93**, 228102.